

RESEARCH ARTICLE SUMMARY

NEURODEVELOPMENT

Oligodendrocyte precursors guide interneuron migration by unidirectional contact repulsion

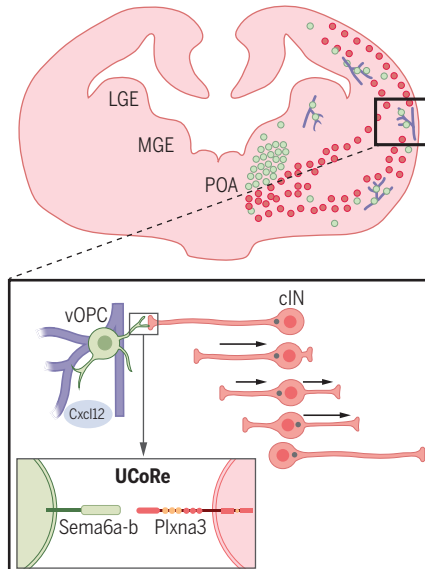
Fanny Lepiemme, Julie Stoufflet, Miriam Javier-Torrent, Gabriel Mazzucchelli, Carla G. Silva*,†, Laurent Nguyen*†

INTRODUCTION: The cerebral cortex is an evolutionarily advanced brain region made of cellular layers tangentially organized into areas that serve higher cognitive functions. During development, most cortical interneurons (hereafter called interneurons) are born in the ventral forebrain, where some progenitors concomitantly generate oligodendrocyte precursor cells (OPCs). OPCs differentiate into oligodendrocytes, the principal functions of which are to wrap axons with myelin to support the rapid saltatory conduction of action potentials and to provide metabolic support to neurons in the postnatal brain. Three distinct populations of OPCs have been identified in the forebrain. These cells are born as successive waves with a defined spatiotemporal pattern, and they all migrate from their birthplace to colonize the brain. The two initial waves are born in the ventral forebrain and named vOPCs. They migrate together with the interneurons toward the cortex, whereas the third OPC wave is generated locally around birth by some progenitors of the cortical wall. Despite their distinct origin, all OPC lineages converge at the transcriptional level, which may reflect their contribution to myelination.

RATIONALE: While migrating, some neural cells promote transient cellular interactions that confer upon them roles additional to those played once integrated into the cortical network. Accordingly, recent studies have reported that some first-wave vOPCs establish synaptic contacts with lineage-related interneurons during early postnatal periods. It is intriguing that a large fraction of the first-wave vOPCs do not contribute to synaptogenesis and are eliminated during the second postnatal week. Here, we assessed whether vOPCs play additional noncanonical functions during brain development by testing whether they cross-talk with interneurons to support their concomitant migration to the cerebral cortex.

RESULTS: We hypothesized that some early functions of vOPCs would rely on their spatiotemporal origin, further defining their field of possible interactions with neighboring cells. Despite being born in shared germinal regions of the ventral forebrain, vOPCs and interneurons occupy mutually exclusive territories while

migrating. Live imaging of both cell populations in brain slices from mouse embryos showed that first-wave vOPCs and interneurons use distinct migration strategies to reach the cortex. Cortical interneurons navigate into organized streams within the parenchyma, whereas first-wave vOPCs prefer migration along blood vessels. The ordered migration of interneurons in cortical streams relies mostly on gradients of chemoattractant molecules such as Cxcl12, to which interneurons are responsive through their expression of the Cxcr4 receptor. This chemokine is also abundantly released by endothelial cells covering the complex and dense network of growing blood vessels that perfuse the ganglionic eminences and later the cortical wall. A long-



Unidirectional contact repulsion provides guidance to migrating interneurons. During embryogenesis, interneurons and first-wave vOPCs are attracted by the Cxcl12 released by blood vessels. By migrating along these structures, first-wave vOPCs prevent contact between interneurons and blood vessels through unidirectional contact repulsion. This mechanism provides guidance to migrating interneurons and relies on the interaction between Sema6a/6b ligands and Plxna3 receptors expressed by first-wave vOPCs and interneurons, respectively. LGE, lateral ganglionic eminence; MGE, medial ganglionic eminence; POA, preoptic area; UCoRe, unidirectional contact-repulsion event.

standing question in the field of brain development is how cortical interneurons cope with different sources, and thus gradients of Cxcl12, to properly navigate within the cortex. Here, we show that first-wave vOPCs, which are also attracted by Cxcl12, migrate along blood vessels and promote unidirectional contact repulsion to repel migrating interneurons from blood vessels. This cellular mechanism, which is not shared by second-wave vOPCs, relies on the expression of the semaphorin 6a/6b by first-wave vOPCs that binds and activates the plexin A3 receptors expressed at the surface of interneurons. This atypical signaling triggers interneuron polarity reversal, preventing them from clustering around blood vessels and allowing them to follow the cortical Cxcl12 gradient (released by intermediate progenitors and meningeal cells) to reach and settle in their cortical layer in a timely manner. Moreover, a prolonged interaction of migrating interneurons with cells that release high levels of Cxcl12, such as endothelial cells, may not only bias their migration directionality but also reduce their motility through a sustained activation of Cxcr4 receptors by Cxcl12, leading to their internalization.

CONCLUSION: During brain development, vOPCs and interneurons are born in the ventral forebrain and migrate concomitantly along tangential routes to reach the cerebral cortex. Here, we show by coupling histological analysis of mouse genetic models with live imaging that, while being responsive to Cxcl12 gradients, both cell populations occupy mutually exclusive forebrain territories enriched in this chemokine. Live-imaging analyses demonstrated that first-wave, but not second-wave, vOPCs perform unidirectional contact repulsion on interneurons. This mechanism steers interneurons away from blood vessels that release Cxcl12, thereby allowing them to follow cortical gradients of this chemokine to later settle in their cortical layer. This mode of contact repulsion is specific to first-wave vOPC-interneuron pairs and distinct from self-repulsion. It relies on the activation of an atypical semaphorin-plexin signaling that induces directional change of interneurons upon their polarity reversal. Whether the specificity of this interaction relies on the degree of interneuron maturation and/or the signaling toolbox of vOPCs belonging in two distinct waves remains to be determined. ■

The list of author affiliations is available in the full article online.

*Corresponding author. Email: Inguyen@uliege.be (L.N.); c.s.gomesdasilva@umcutrecht.nl (C.G.S.)

Cite this article as F. Lepiemme et al., *Science* **376**, eabn6204 (2022). DOI: 10.1126/science.abn6204

†These authors contributed equally to this work.

S READ THE FULL ARTICLE AT
<https://doi.org/10.1126/science.abn6204>

RESEARCH ARTICLE

NEURODEVELOPMENT

Oligodendrocyte precursors guide interneuron migration by unidirectional contact repulsion

Fanny Lepiemme¹, Julie Stoufflet¹, Míriam Javier-Torrent¹, Gabriel Mazzucchelli², Carla G. Silva^{1*}†, Laurent Nguyen^{1*}†

In the forebrain, ventrally derived oligodendrocyte precursor cells (vOPCs) travel tangentially toward the cortex together with cortical interneurons. Here, we tested in the mouse whether these populations interact during embryogenesis while migrating. By coupling histological analysis of genetic models with live imaging, we show that although they are both attracted by the chemokine Cxcl12, vOPCs and cortical interneurons occupy mutually exclusive forebrain territories enriched in this chemokine. Moreover, first-wave vOPC depletion selectively disrupts the migration and distribution of cortical interneurons. At the cellular level, we found that by promoting unidirectional contact repulsion, first-wave vOPCs steered the migration of cortical interneurons away from the blood vessels to which they were both attracted, thereby allowing interneurons to reach their proper cortical territories.

Oligodendrocytes differentiate from oligodendrocyte progenitor cells (OPCs) and populate the entire central nervous system. After birth, they progressively wrap axons to support rapid saltatory conduction of action potentials as well as to provide metabolic support to neurons through axo-myelinic channels (1). Some OPCs convert into neural/glial antigen 2 (NG2)-expressing glia, which is the most proliferative pool of cells in the mature brain (2). These cells also form synapses with neurons (3–5). OPCs from different central nervous system regions are genetically distinct, and several intermediates coexist during development (6), but some further converge into similar transcriptional states after birth (7). In the forebrain, OPCs have multiple origins and are generated in successive “spatiotemporal waves” that populate the cortex from embryonic development onward (8). The two first OPC waves are ventrally derived OPCs (vOPCs) that are produced in the ventral forebrain and are followed by a perinatal wave born in the cerebral cortex, which gradually expands and outnumbers the others (8). Although the second and third OPC waves mainly contribute to axon myelination, the function of the first-wave vOPC cohort remains elusive. This cell population was first thought to be transient and eliminated at birth (8), but despite undergoing massive cell death, recent single-cell analyses showed its maintenance and persistence in some brain regions during

adulthood (7). Most first-wave vOPCs share common embryonic origins with cortical interneurons (hereafter referred as interneurons). They are born from progenitors of the medial ganglionic eminence and the preoptic area, where genetic cross-inhibitory mechanisms control the balanced generation of interneurons and first-wave vOPCs. The expression of some Distal-less (Dlx) homeobox transcription factors drives interneuron fate by repressing the OPC gene Oligodendrocyte Transcription Factor 2 (*Olig2*) (9), whereas Oligodendrocyte Transcription Factor 1 (*Olig1*) expression promotes the specification of first-wave vOPCs and prevents the acquisition of an interneuron fate by repressing *Dlx1/2* expression (10). Some first-wave vOPCs from the preoptic area (*Dbx1*⁺) or from the medial ganglionic eminence (*Nkx2.1*⁺) cluster with their lineage-related interneurons in the cortex of newborn mice, where they form transient synapses before engaging into myelination of specific local circuits (5, 11). During embryogenesis, vOPCs and interneurons migrate concomitantly into the cerebral cortex (8, 12), a process during which these cells may interact and cooperate. We tested this hypothesis by performing live imaging on organotypic forebrain slices from transgenic mice to analyze the distribution and dynamic behavior of vOPCs and interneurons. We first showed that, despite coexisting in time and space, these cells occupy different territories and invade the cortex using distinct migration modes and paths. The elimination of first-wave vOPCs from the early forebrain results in changes of interneuron distribution and migration, supporting the existence of a functional cross-talk between these two cell types that starts at the onset of corticogenesis. At the cellular level, we found that first- but not second-wave vOPCs repel interneurons by

a process that we named unidirectional contact repulsion. This atypical behavior contributes to the guidance of interneurons in streams, preventing them from clustering around blood vessels. vOPCs and interneurons are both attracted by the chemokine Cxcl12 released by blood vessels. However, vOPCs are the only ones to move along blood vessels, where they also divide (13). Here, we show that the forebrain depletion of some first-wave vOPCs results in interneuron clustering around blood vessels by locally increasing Cxcl12 availability. Altogether, our data demonstrate that by inducing unidirectional contact repulsion, first-wave vOPCs play a transient role in supporting interneuron migration in the developing brain. Unidirectional contact repulsion is thus a strategy allowing first-wave vOPCs and interneurons, which are both responsive to a common chemoattractant, to progress in a coordinated fashion on shared forebrain territories.

Results

Forebrain spatial segregation of interneurons and vOPCs

We analyzed the dynamic distribution pattern of first-wave vOPCs (platelet-derived growth factor receptor A, *Pdgfra*⁺) (8) and most interneurons (calbindin⁺) that migrate in the early forebrain (14). At embryonic day 11.5 (E11.5), both cell types mostly distribute into nonoverlapping subpallial territories (Fig. 1, A to D). First-wave vOPCs populate the germinal zones of the medial ganglionic eminence/preoptic area, whereas interneurons are distributed throughout their subventricular and mantle zones (SVZ and MAZ, respectively) (Fig. 1, A and B). At E13.5, first-wave vOPCs accumulate in the SVZ and along the MAZ against a stream of migrating interneurons (Fig. 1, E to H). Calbindin⁺ interneurons born in the medial ganglionic eminence organize into a deep migratory stream (DMS), and those derived from the preoptic area form a superficial migratory stream (SMS) (Fig. 1E) (15). Most first-wave vOPCs do not integrate these migratory streams, suggesting that during early embryonic periods, first-wave vOPCs and interneurons are spatially segregated in the subpallium. This was further confirmed by the analysis of maximum fluorescence intensities and relative number of cells expressing *Pdgfra* or calbindin at E11.5 (Fig. 1, C and D) and at E13.5 (Fig. 1, G and H), supporting the spatial segregation of first-wave vOPC and interneuron populations in the ventral forebrain. We showed that vOPCs occupying the medial ganglionic eminence/preoptic area territory above the DMS mainly arise from *Nkx2.1*⁺ ($87.72 \pm 5.04\%$) and *Dbx1*⁺ ($31.23 \pm 2.05\%$) progenitors (Fig. 1, I to L). We next analyzed the distribution of first-wave vOPCs and interneurons in the cortical wall of E13.5 embryos and followed their migration in transgenic mice [Dlx5,6:Cre-GFP]

¹Laboratory of Molecular Regulation of Neurogenesis, GIGA-Stem Cells and GIGA-Neurosciences, Interdisciplinary Cluster for Applied Genoproteomics (GIGA-R), University of Liège, CHU Sart Tilman, 4000 Liège, Belgium. ²Laboratory of Mass Spectrometry, MolSys Research Unit, Liege University, Liege, Belgium.

*Corresponding author. Email: Nguyen@uliege.be (L.N.); c.s.gomesdasilva@umcutrecht.nl (C.G.S.)

†These authors contributed equally to this work.

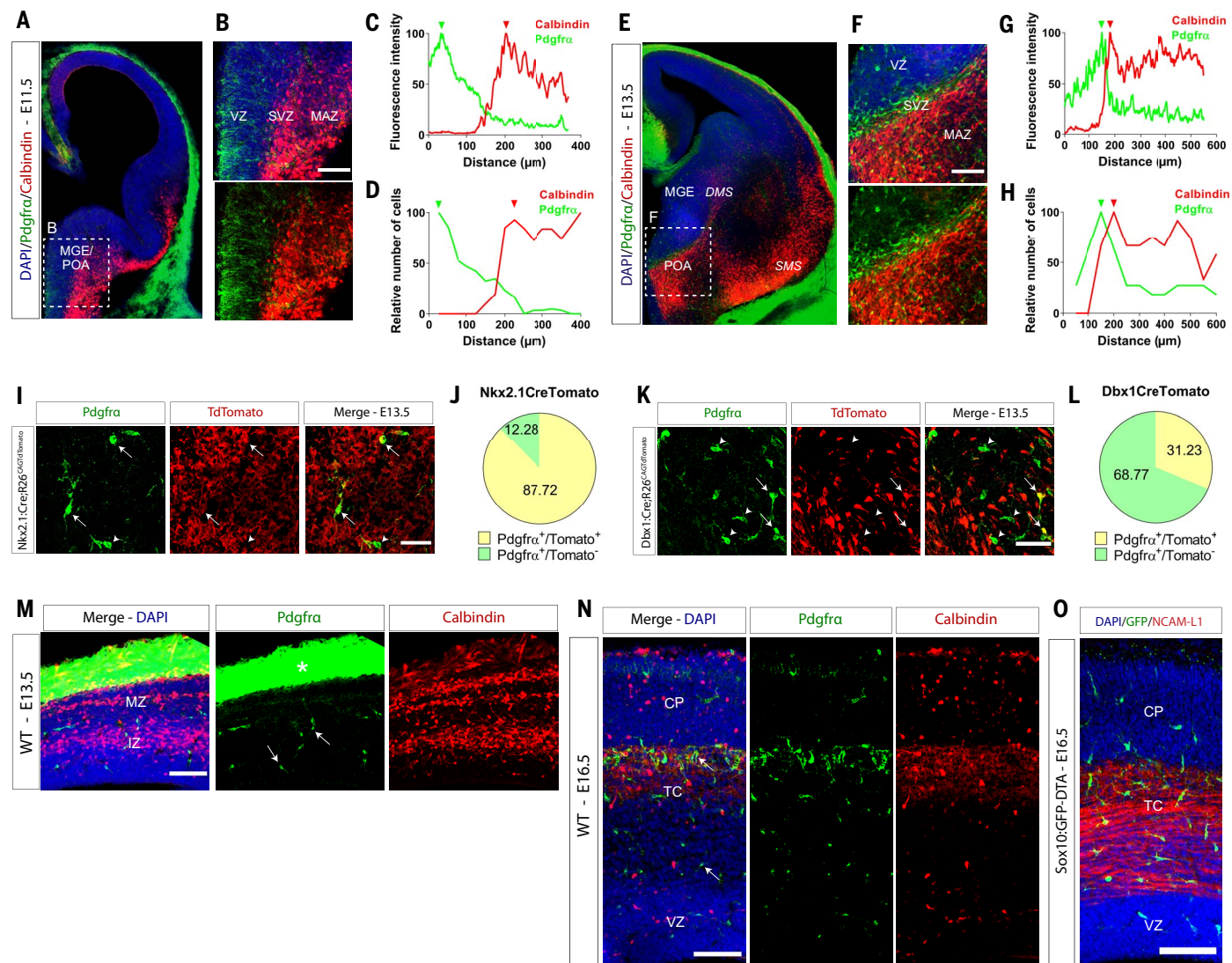


Fig. 1. vOPCs and interneurons occupy distinct territories. (A and B) Immunolabeling of first-wave vOPCs (Pdgfra^+ , green) and interneurons (Calbindin^+ , red) in a coronal brain slice of a wild-type (WT) E11.5 mouse embryo (cells never coexpressed both markers). First-wave vOPCs localize mostly in VZ and interneurons in SVZ and MAZ of medial ganglionic eminence/preoptic area. Nuclei were counterstained with 4',6-diamidino-2-phenylindole (DAPI) (blue). (C) Fluorescence intensity distribution of Pdgfra and Calbindin immunolabelings within the magnified area represented in (B) from VZ to MAZ. Maximum fluorescence intensities (MFIs) are indicated by color-matching arrowheads. (D) Distribution of relative numbers of Pdgfra^+ and Calbindin^+ cells observed in (B). Maximum relative numbers are indicated by color-matching arrowheads. (E) Immunolabeling of first-wave vOPCs and interneurons in a coronal brain slice of a WT E13.5 mouse embryo. (F) Magnified regions of medial ganglionic eminence and preoptic area are squared in (E), where first-wave vOPCs localize across the VZ/SVZ with accumulation in the SVZ, and interneurons in the MAZ of the medial ganglionic eminence and preoptic area. Nuclei were counterstained with DAPI (blue). (G) Fluorescence intensity distribution of Pdgfra and Calbindin immunolabelings within the magnified area represented in (F). MFIs are indicated by color-matching arrowheads. (H) Distribution of relative numbers of Pdgfra^+ and Calbindin^+ cells observed in (F). Maximum relative numbers are indicated by color-matching arrowheads for Pdgfra^+ (green) or Calbindin^+ (red) cells. (I) Lineage tracing of Pdgfra^+ first-wave vOPCs in $\text{Nkx2.1:Cre;R26}^{\text{GAGTdTTomato}}$ in a medial ganglionic eminence region

above the DMS from E13.5 embryos. White arrows indicate Pdgfra^+ first-wave vOPCs generated by Nkx2.1^+ progenitors and the white arrowhead indicates a Pdgfra^+ first-wave vOPC of other origin. (J) Proportion of Pdgfra^+ first-wave vOPCs originating from Nkx2.1^+ progenitors (yellow) or from other progenitors (green). (K) Lineage tracing of Pdgfra^+ first-wave vOPCs in $\text{Dbx1:Cre;R26}^{\text{GAGTdTTomato}}$ in a medial ganglionic eminence region above DMS from E13.5 embryos. White arrows indicate Pdgfra^+ first-wave vOPCs generated from Dbx1^+ progenitors, and white arrowheads indicate Pdgfra^+ first-wave vOPCs of other origin. (L) Proportion of Pdgfra^+ cells originating from Dbx1^+ progenitors (yellow) or from other progenitors (green). (M) Distribution of first-wave vOPCs (Pdgfra^+ , green) and interneurons (Calbindin^+ , red) in the cortex of a WT E13.5 embryo (25- μm Z-stack). Interneurons distribute within two migratory streams located in the MZ and IZ. White arrows indicate first-wave vOPCs that are distributed randomly. Nuclei were counterstained with DAPI (blue). The asterisk shows immunolabeling of meninges that are Pdgfra^+ . (N) Distribution of vOPCs (Pdgfra^+ , green) and interneurons (Calbindin^+ , red) in the cortical plate (CP) of an E16.5 WT embryo. Interneurons largely populate the CP, whereas vOPCs accumulate under the CP and above the VZ. Nuclei were counterstained with DAPI (blue). (O) Immunolabeling of a brain section of a E16.5 Sox10:GFP-DTA embryo showing the accumulation of vOPCs (Pdgfra^+ , green) on NCAM-L1 $^+$ thalamocortical fibers (NCAM-L1, red). Nuclei were counterstained with DAPI (blue). Scale bars: (I) and (K), 50 μm ; (B), (F), (M), (N), and (O), 100 μm . MGE, medial ganglionic eminence; POA, preoptic area; SMS, superficial migratory stream; TC, thalamocortical fibers.

for interneurons, and *Sox10*:*loxGFP-STO*^{lox}-DTA (further referred as *Sox10*:GFP-DTA) for vOPCs, which largely coexpress calbindin and *Pdgfra*, respectively; fig. S1, A to C]. Although interneurons migrate within two main tangential streams located in the marginal zone (MZ) and the intermediate zone (IZ), vOPCs show erratic distribution within the cortical wall (Fig. 1M and movies S1 and S2). At the cellular level, both interneurons and vOPCs undergo saltatory migration, but vOPCs move at a slower speed as a result of a reduced nucleokinesis frequency and amplitude (fig. S1, D to F) combined with longer pausing time of their nucleus (fig. S1G). At E16.5, numerous interneurons undergo intracortical dispersion, whereas most vOPCs accumulate under the cortical plate, where NCAM-L1⁺ thalamocortical fibers extend (Fig. 1, N and O).

Depletion of vOPCs alters forebrain interneuron distribution

We next wondered whether the spatial segregation of interneurons and first-wave vOPCs in the forebrain results from responsiveness to different cues or if it arises from their mutual interaction. To investigate these two possibilities, we crossed *Pdgfra*:Cre^{ERT} and *Sox10*:GFP-DTA mice to generate embryos devoid of first-wave vOPCs (OPC-depleted embryos) upon successive (E11.5 and E12.5) intraperitoneal injections of tamoxifen in pregnant dams. The depletion of first-wave vOPCs was confirmed at E13.5 and E14.5 (Fig. 2A and fig. S2, A and B). This procedure did not induce bystander cell death, changes in ganglionic eminence progenitor proliferation, or changes in interneuron numbers (fig. S2, C to I). The forebrain of E14.5 OPC-depleted embryos showed enlarged DMS as a

result of an increased dispersion of calbindin⁺ interneurons (Fig. 2, B and C). Analysis of the dorsal forebrain of E13.5 and E16.5 embryos showed a reduced number of calbindin⁺ interneurons into cortical streams upon first-wave vOPC depletion (Fig. 2, D to G). The acute loss of first-wave vOPCs did not prevent later-born second-wave vOPCs from invading the cortical wall of OPC-depleted embryos at E16.5 (fig. S2, J and K). We next crossed OPC-depleted mice with *Dlx5,6*:Cre-GFP mice to generate green fluorescent protein-positive (GFP⁺) cortical interneuron (cIN)-OPC-depleted embryos and followed the migration of GFP⁺ interneurons, which included most future cortical interneuron subtypes (Fig. 2A). The number of GFP⁺ interneurons in E13.5 GFP⁺cIN-OPC-depleted embryos was reduced in the cortical wall, suggesting that the loss of first-wave vOPCs affects

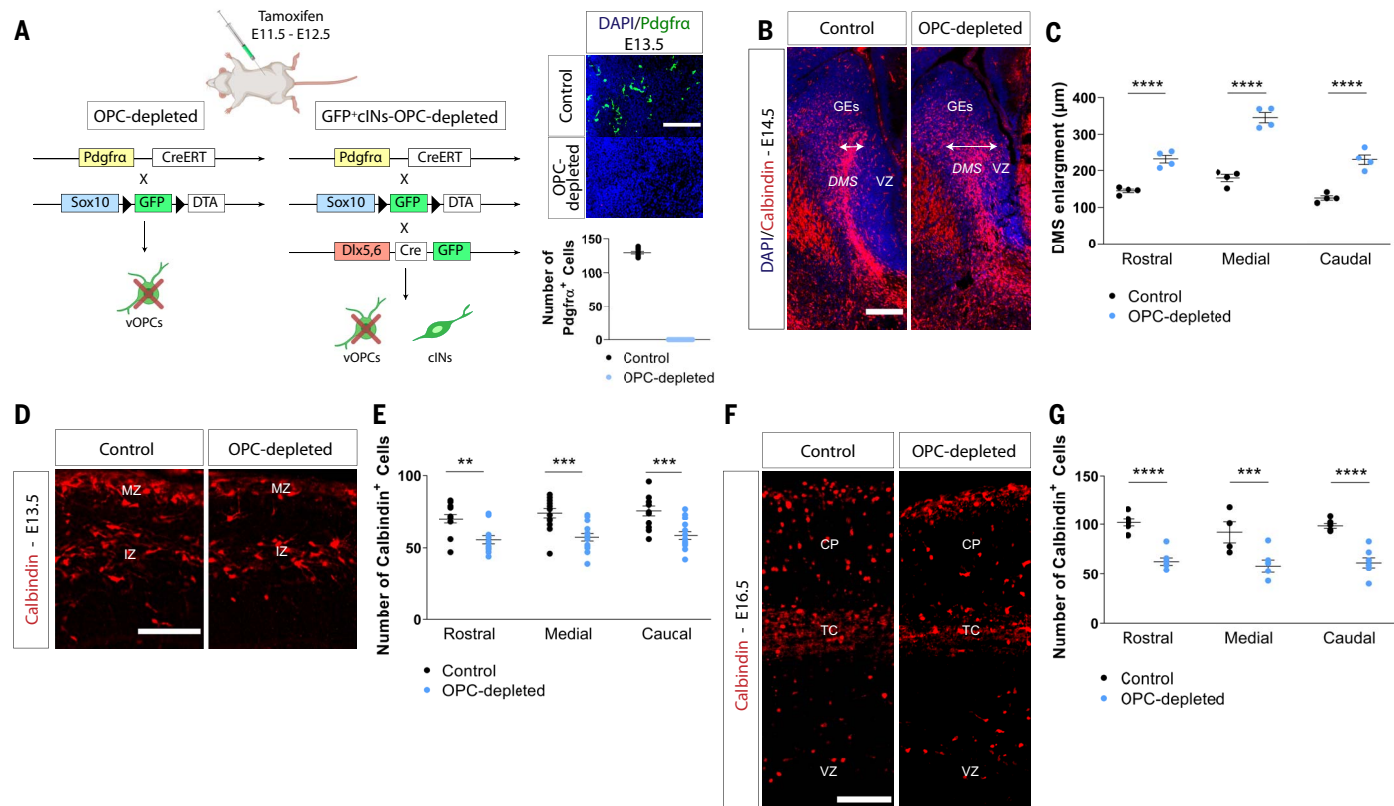


Fig. 2. Depletion of first-wave vOPCs alters interneuron distribution in the forebrain. (A) Mouse breeding strategies to deplete *Pdgfra*⁺:*Sox10*⁺ first-wave vOPCs through conditional expression of DTA upon tamoxifen injection (OPC-depleted) and to visualize *Dlx5,6*-GFP⁺ interneurons (GFP⁺cIN-OPC-depleted). Immunolabeling of brain slices from E13.5 siblings *Pdgfra*:Cre^{ERT} (Control) and *Pdgfra*:Cre^{ERT};*Sox10*:GFP-DTA (OPC-depleted) embryos shows complete loss of first-wave vOPCs (green) in the medial ganglionic eminence/preoptic area after tamoxifen injection in OPC-depleted embryos. Right, immunolabeling and quantification ($n = 13$ embryos, 100% of depletion). Nuclei were counterstained with DAPI. (B) Immunolabeling of interneurons (red) in the subpallium of E14.5 control and OPC-depleted embryos. Migrating interneurons are organized into a DMS stream, which is enlarged in OPC-depleted embryo at three rostrocaudal levels. (C) Quantifications of DMS width in its upper part at three rostrocaudal levels, as illustrated in (B) ($n = 4$ embryos;

**** $P < 0.0001$, two-way ANOVA). (D) Immunolabeling of interneurons (red) in the cortical wall of E13.5 control and OPC-depleted embryos. The number of migrating interneurons in the MZ and IZ streams is decreased upon first-wave vOPC depletion. (E) Quantification of the number of interneurons (red) in rostrocaudal regions of the cortex of E13.5 control and OPC-depleted embryos ($n = 13$ to 14 embryos, ** $P = 0.0024$, *** $P = 0.0004$, *** $P = 0.0003$, respectively, two-way ANOVA). (F) Immunolabeling of interneurons (red) in the cortical wall of E16.5 control and OPC-depleted embryos. The number of interneurons (red) is decreased in the CP. (G) Quantification of the number of interneurons (red) in the rostrocaudal regions of the cortex of E16.5 control and OPC-depleted embryos ($n = 6$ to 7 embryos; **** $P < 0.0001$, *** $P = 0.0007$, *** $P < 0.0001$, two-way ANOVA). Scale bars: (A) and (D), 50 μm; (F), 100 μm; (B), 200 μm. GE, ganglionic eminence.

the migration of most interneurons (fig. S3, A and B). This was further supported by the ventral accumulation of a cohort of 5-ethynyl-2'-deoxyuridine (EdU)-positive interneurons born at E11.5 in the forebrain of E13.5 OPC-depleted embryos (fig. S3, C to E). Despite the progressive increase of vOPC numbers generated by the second wave in OPC-depleted cortex (where most first-wave vOPCs had been eliminated), the number of interneurons in the cortical wall remained decreased at E18.5, just before the death of embryos (fig. S3, H and I). This defect seems specific to interneurons because cortical distribution of microglia, which migrate concomitantly with both interneurons and vOPCs, remained unchanged at E13.5 (fig. S3, J and K). Moreover, depleting interneurons by expressing diphtheria toxin subunit A (DTA) in Dlx5,6⁺ cells (Dlx5,6:Cre-GFP;R26:DTA) had no effect on the number or localization of vOPCs within the cortical parenchyma (fig. S3, L to N). These results contrast with those observed with OPCs generated dorsally around birth, the generation of which is impaired upon loss of interneurons (16). Altogether, these results suggest that first-wave vOPCs selectively influence the forebrain distribution and sorting of interneurons into the cortical wall.

vOPCs prevent interneuron–blood vessel interaction

During late development, vOPCs migrate in close association to blood vessels (13). We observed that during the early developmental stages, when the cortical wall is less vascularized, first-wave vOPCs migrate independently of blood vessels with similar dynamics, suggesting an intrinsic regulation of their migration (fig. S4, A to E). The percentage of vOPCs migrating on blood vessels increases as cortogenesis proceeds, following the spatiotemporal progression of cortical angiogenesis (17) (E13.5: 52.46 ± 4.45%; E16.5: 77.52 ± 7.86%; fig. S4, A and F). Our analysis may underestimate the blood vessel coverage by vOPCs because these cells extend thin processes between blood vessels while migrating, which are difficult to image by time-lapse recordings. Although interneurons do not preferentially migrate on blood vessels, they can be detected in their vicinity (18).

We tested whether the impaired forebrain distribution of interneurons upon depletion of first-wave vOPCs results from a change in their migratory behavior. We crossed OPC-depleted mice with Dlx5,6:Cre-GFP mice to generate GFP⁺cIN-OPC-depleted embryos and follow the migration of GFP⁺ interneurons (Fig. 2A). Live imaging of organotypic brain slices from E13.5 embryos showed a reduction of cortical invasion by interneurons in GFP⁺cIN-OPC-depleted embryos (Fig. 3, A and B, and movie S3). In brain slices from E13.5 GFP⁺cIN-OPC-depleted embryos, interneurons were migrating more slowly (Fig. 3C) and closer to isolectinB4-

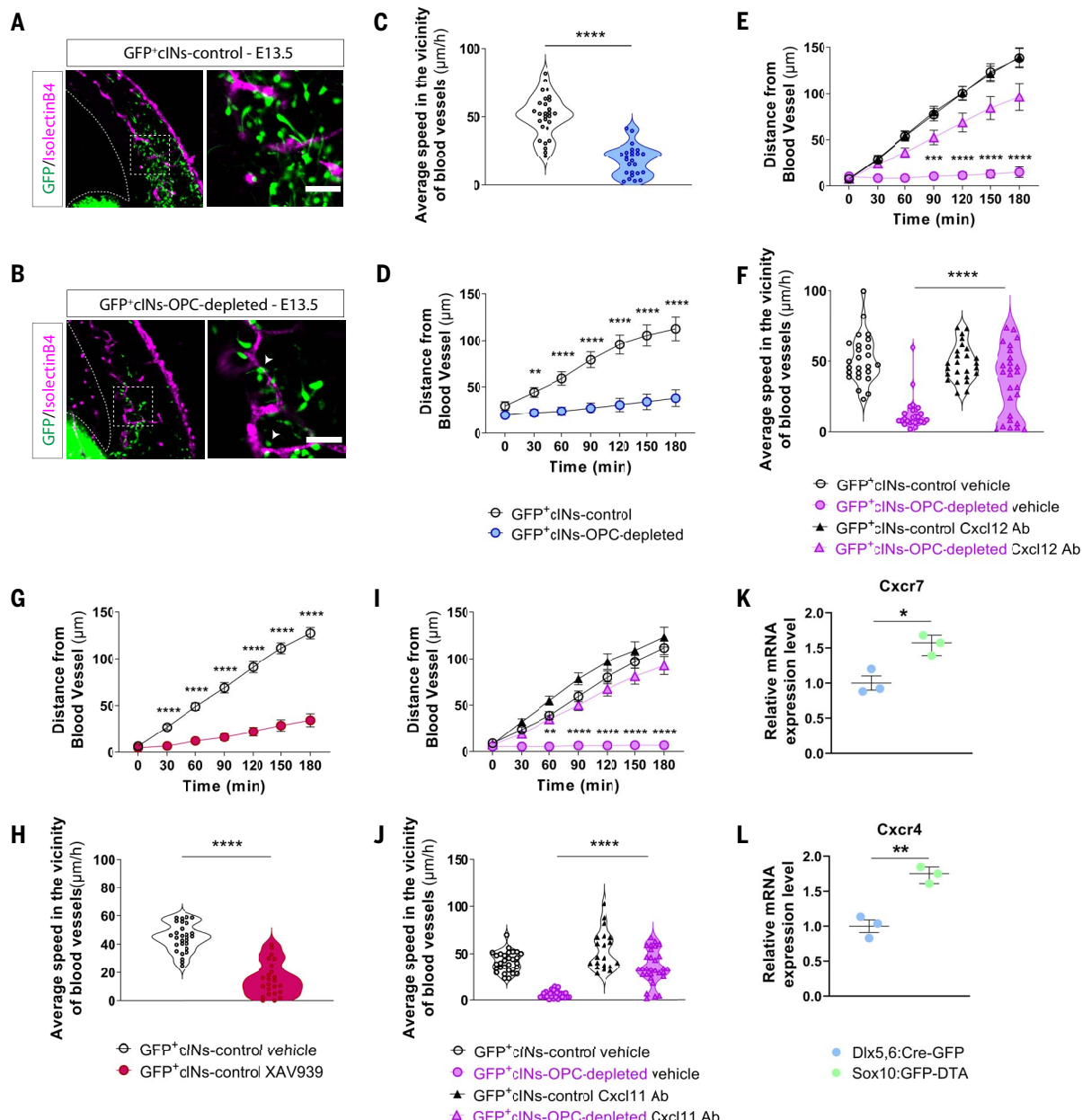
labeled blood vessels in the cortical wall (Fig. 3D) and in the ventral forebrain (fig. S3, C to G). At E13.5, the migration parameters of interneurons in cortical parenchyma devoid of blood vessels were comparable between GFP⁺cIN-OPC-depleted and control cortices (fig. S5, A to D), suggesting that changes in interneuron migration between genotypes result from a lack of blood vessel coverage by first-wave vOPCs. In the forebrain, blood vessels are an important source of Cxcl12 (13) (fig. S5, E and F), which attracts vOPCs that express the C-X-C chemokine receptor 4 (Cxcr4) upon activation of Wnt signaling (13). Although loss of Ng2⁺ OPCs results in an impaired blood vessel network before birth (19), the vasculature was not affected at E13.5 upon first-wave vOPC depletion in OPC-depleted embryos (fig. S5, G to S). This was further supported by a proteomic analysis of the cortical wall that did not indicate specific molecular changes associated with blood vessels (despite detected proteomic changes associated with the loss of first-wave vOPCs) (fig. S5, T and U). Moreover, we did not detect a change of Cxcl12 amount in cortical extracts from E13.5 OPC-depleted embryos compared with their controls (fig. S5V and table S4).

The ordered migration of interneurons in cortical streams relies mostly on gradients of chemoattractant molecules, including Cxcl12, to which interneurons are responsive through their expression of Cxcr4 (18, 20–22). Therefore, we postulated that a loss of blood vessel coverage by first-wave vOPCs in E13.5 OPC-depleted embryos would free a local source of Cxcl12, resulting in attraction and rerouting of interneurons toward cortical blood vessels. To test this hypothesis, we incubated organotypic brain slices from E13.5 GFP⁺cIN-OPC-depleted embryos with Cxcl12-blocking antibodies (Cxcl12 Ab) and measured the distance traveled by interneurons after contacting a blood vessel. We found that interneurons spent less time interacting with blood vessels and migrated farther away from these structures upon initial contact in GFP⁺cIN-OPC-depleted brain slices incubated with Cxcl12 Ab (Fig. 3E and movie S4). These changes correlated with an increased average speed of interneurons (Fig. 3F). Incubation of control brain slices (GFP⁺cIN-control) with Cxcl12 Ab did not modify the distance traveled by interneurons from blood vessels (Fig. 3E). The average speed was also similar between Cxcl12 treatment conditions (Fig. 3F). Altogether, these results suggest that the coverage of blood vessels by first-wave vOPCs prevents the Cxcl12-mediated interaction between interneurons and blood vessels. To further support this hypothesis, we induced first-wave vOPC detachment from the vasculature by blocking Wnt signaling with XAV939 in control brain slices (13). This pharmacological induction of first-wave vOPC detachment led to an ac-

cumulation of interneurons around blood vessels that were migrating more slowly (Fig. 3, G and H, and movie S5). Blood vessels also release Cxcl11 (23, 24) that selectively binds to C-X-C chemokine receptor type 7 (Cxcr7), which acts as a Cxcl12 scavenger and maintains Cxcr4 activation by preventing its internalization (25–27). We thus blocked Cxcl11 with antibodies (Cxcl11 Ab) and found that it rescued interneuron migration in GFP⁺cIN-OPC-depleted cortices, likely by preventing Cxcr4 internalization upon blood vessel-released Cxcl12 activation (Fig. 3, I and J). Furthermore, we found that first-wave vOPCs express higher levels of both Cxcr4 and Cxcr7 compared with interneurons (Fig. 3, K and L), which may help them to migrate more efficiently than interneurons along blood vessels.

vOPCs modulate interneuron migration by unidirectional contact repulsion

We found that first-wave vOPC depletion impairs the distribution and migration of concomitantly born interneurons in forebrain parenchyma, including along its blood vessels, suggesting the existence of a cross-talk between first-wave vOPCs and interneurons. Culturing medial ganglionic eminence explants from E13.5 Nkx2.1:Cre; R26^{CAGTdTmato} embryos [containing TdTomato⁺ (Tom⁺) interneurons] with dissociated preoptic area isolated from E13.5 Sox10:GFP-DTA embryos (enriched in GFP⁺ first-wave vOPCs) in compartmented dishes did not change the migration of Tom⁺ interneurons around their medial ganglionic eminence core explants (Fig. 4, A to H). This suggests that factors released by first-wave vOPCs in culture do not influence interneuron migration. We next investigated whether contact between interneurons and first-wave vOPCs would influence their respective migration behavior. To test this, we cocultured medial ganglionic eminence and preoptic area explants (with or without first-wave vOPCs), which include isolectinB4-labeled cells (Fig. 4I and fig. S5W). After 48 hours of culture, we observed a reduction of preoptic area explant invasion by Tom⁺ interneurons when they included first-wave vOPCs (Fig. 4, J to L). This suggested that first-wave vOPCs prevent preoptic area invasion by interneurons. At the cellular level, live imaging showed that first-wave vOPC-interneuron contact is a multistep event during which first-wave vOPC extends one branch recognizing the interneuron leading process on its growth cone-like structure, followed by polarity reversal and migration of interneuron, without altering first-wave vOPC migration (Fig. 4M and movie S6). This unidirectional contact repulsion (UCoRe) ended on average 78.6 ± 6.11 min after the initial contact (Fig. 4N) and was highly specific, only occurring between first-wave vOPCs and interneurons (Fig. 4, O to R). Unidirectional contact

**Fig. 3. First-wave vOPC depletion leads to changes in interneuron migration**

behavior. (A and B) Images showing the distribution of interneurons (green) around blood vessels (purple) on organotypic brain slices from E13.5 GFP⁺cIN-control (A) and GFP⁺cIN-OPC-depleted embryos (B). Right panels are magnified images of corresponding left panels. White arrowheads in (B) indicate interneurons located in the vicinity of blood vessels. (C) Distribution of average migration speed of interneurons moving along cortical blood vessels in E13.5 GFP⁺cIN-control and GFP⁺cIN-OPC-depleted brain slices ($n = 25$ to 28 cells; **** $P < 0.0001$, unpaired t test). (D) Histogram of the distance traveled by interneurons, starting from their closest position to blood vessels, in brain slices from E13.5 GFP⁺cIN-control or GFP⁺cIN-OPC-depleted embryos. Time 0 corresponds to initial contact of interneuron with a blood vessel ($n = 23$ cells; ** $P = 0.0048$ after 30 min, **** $P < 0.0001$ after 60 to 180 min, two-way ANOVA). (E) Histogram of the distance traveled by interneurons, starting from their closest position to blood vessels, in brain slices from E13.5 GFP⁺cIN-control or from GFP⁺cIN-OPC-depleted embryos ($n = 24$ to 25 cells; *** $P = 0.0006$ after 90 min, **** $P < 0.0001$ after 120 to 180 min, two-way ANOVA). (F) Distribution of average migration speed of interneurons moving along cortical blood vessels on Cxcl12 Ab-treated or vehicle-treated organotypic brain slices from E13.5 GFP⁺cIN-control or GFP⁺cIN-OPC-depleted embryos ($n = 3$ samples; * $P = 0.014$ and ** $P = 0.0029$, respectively, unpaired t test). Scale bars: (A) and (B), 50 μm .

brain slices from E13.5 GFP⁺cIN-control and GFP⁺cIN-OPC-depleted embryos ($n = 25$ to 26 cells; *** $P < 0.0001$, one-way ANOVA). (G) Histogram of the displacement of interneurons, starting from their closest position to blood vessels, on brain slices from E13.5 GFP⁺cIN-control vehicle-treated and GFP⁺cIN-control XAV939-treated embryos ($n = 23$ to 28 cells; *** $P < 0.0001$ after 30 to 180 min, two-way ANOVA). (H) Distribution of average migration speed of interneurons moving along cortical blood vessels on organotypic brain slices from E13.5 GFP⁺cIN-control vehicle-treated or GFP⁺cIN-control XAV939-treated embryos ($n = 24$ to 28 cells; **** $P < 0.0001$, unpaired t test). (I) Histogram of the distance traveled by interneurons, starting from their closest position to blood vessels, in brain slices from E13.5 GFP⁺cIN-control or GFP⁺cIN-OPC-depleted embryos ($n = 30$ cells; ** $P = 0.0069$ after 60 min, **** $P < 0.0001$ after 90 to 180 min, two-way ANOVA). (J) Distribution of average migration speed of interneurons moving along cortical blood vessels on Cxcl11 Ab-treated or vehicle-treated organotypic brain slices from E13.5 GFP⁺cIN-control or GFP⁺cIN-OPC-depleted embryos ($n = 30$ cells; *** $P < 0.0001$, one-way ANOVA). (K and L) Dot plots of relative mRNA expression levels of Cxcr7 and Cxcr4 in first-wave vOPCs, compared with interneurons ($n = 3$ samples; * $P = 0.014$ and ** $P = 0.0029$, respectively, unpaired t test).

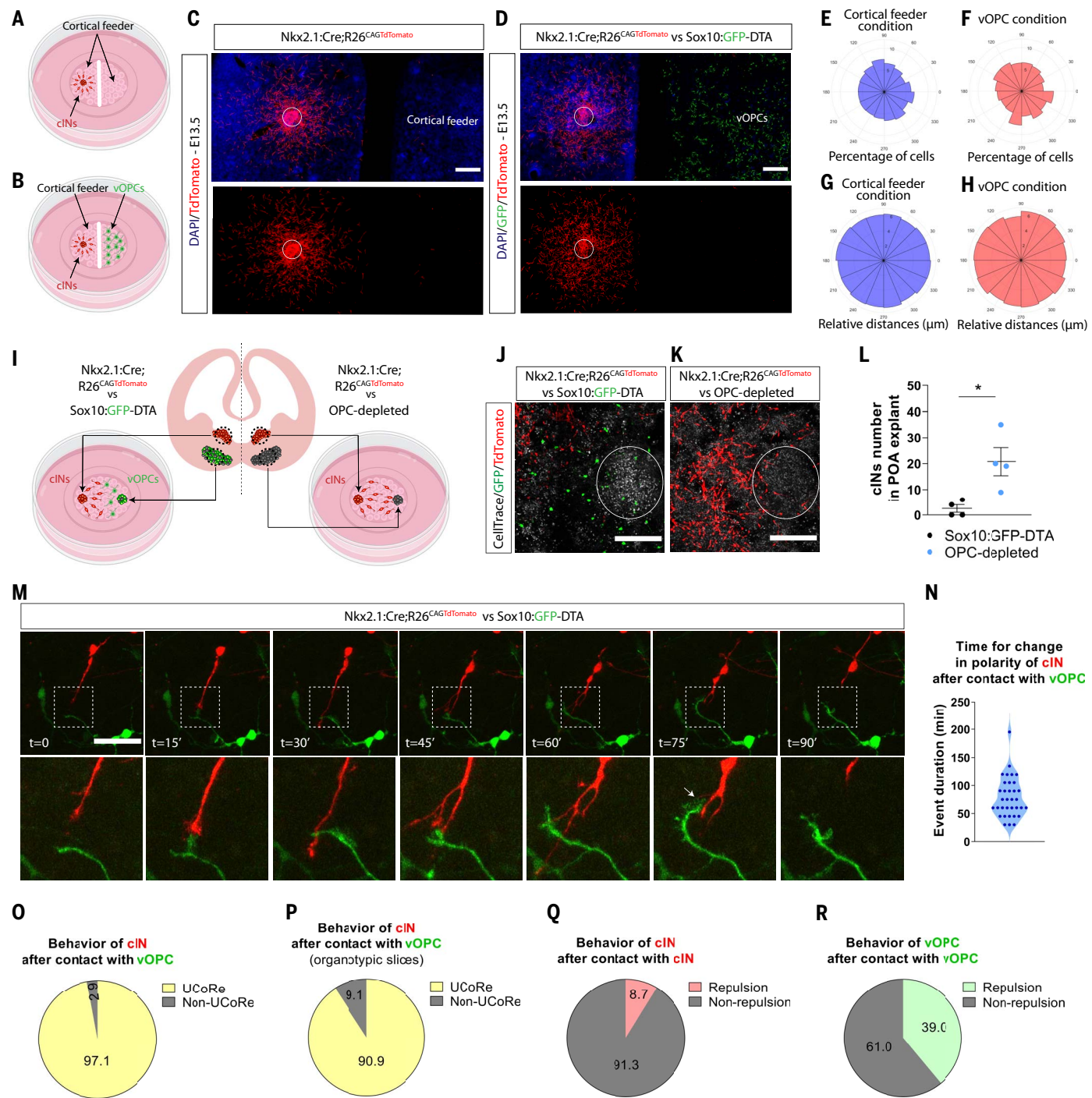


Fig. 4. Analysis of first-wave vOPC-interneuron interactions. (A and B) Experimental culture setup to test whether first-wave vOPC secretome influences interneuron migration. (C and D) Images showing cocultures of interneurons with or without first-wave vOPCs, as depicted in (A) and (B). (E to H) Phase histograms showing the cell percentage [(E) and (F)] or the distance traveled by interneurons [(G) and (H)] from the explant core in the culture as depicted in (A) and (B). (I) Experimental in vitro setup to assess the ability of interneurons (red) to invade the preoptic area that contains or does not contain first-wave vOPCs (green). (J and K) Representative images of medial ganglionic eminence-derived explants isolated from organotypic brain slices of E13.5 Nkx2.1:Cre; R26^{CAGTdTmato} embryos cocultured with preoptic area-derived explants obtained from organotypic brain slices of E13.5 Sox10:GFP-DTA (J) or OPC-depleted (K) embryos. (L) Absolute numbers of

interneurons that invade preoptic area-derived explants from Sox10:GFP-DTA or OPC-depleted embryos ($n = 4$ explants; $*P = 0.0286$, Mann-Whitney test). (M) Time-lapse sequence showing the interaction (white arrow) between an interneuron (red) and a first-wave vOPC (green). (N) Violin plot of the timing of unidirectional contact repulsion (UCoRe) when interneurons contact first-wave vOPCs (78.60 ± 6.11 min; $n = 34$ interactions). (O and P) Pie charts reporting the frequency of UCoRe or non-UCoRe behaviors among interneuron-first-wave vOPC contacts in explant cultures [(O); $n = 35$ cells] or in situ in organotypic slices [(P); $n = 11$ cells]. (Q and R) Pie charts of the frequency of repulsive and neutral behaviors upon interneuron-interneuron [(Q); $n = 46$ cells] or first-wave vOPC-first-wave vOPC [(R); $n = 41$ cells] contacts. Scale bars: (J), (K), and (M), 200 μm; (C) and (D), 500 μm. UCoRe, unidirectional contact-repulsion event.

repulsion is a distinct mode of cell repulsion compared with the mutual ones occurring between pairs of first-wave vOPCs (39.0% of the recorded contacts) or interneurons (8.7% of the recorded contacts) that never experienced polarity reversal (Fig. 4, Q and R). This mode of cell repulsion likely occurs *in vivo* as it guides interneuron migration in cortical regions from organotypic slices in the vicinity of or at a distance from blood vessels through dynamic branching of first-wave vOPCs (Fig. 4P and movies S7 and S8).

We next performed coculture of E16.5 lateral ganglionic eminence explants containing second-wave vOPCs (*Sox10:venus/GFP*; green) with homochronic medial ganglionic eminence explants (*Nkx2.1:Cre;R26^{CAGTdTmato}*; red) containing interneurons or homochronic caudal ganglionic eminence explants (*Dlx5,6:Cre-GFP*; *R26^{CAGTdTmato}*, yellow) containing interneurons. In both cultures, second-wave vOPCs did not promote unidirectional contact repulsion to most medial ganglionic eminence- or caudal ganglionic eminence-derived interneurons (fig. S6, A to D).

Unidirectional contact repulsion relies on atypical semaphorin-plexin signaling

To identify the molecular mechanism underlying unidirectional contact repulsion, we performed enrichment analysis of a gene set obtained by RNA sequencing of GFP⁺ interneurons purified by fluorescence-activated cell sorting (FACS) from E13.5 *Dlx5,6:Cre-GFP* embryos (28). We ran gene ontology (GO) analysis (29) to identify the GO term related to chemotaxis and refined the analysis by selecting genes coding for transmembrane receptors and membrane-bound signaling molecules (table S1). Among the 10 genes showing the highest enrichment in interneurons, we found several members of the Eph-ephrin and Plexin (Plxn)-Semaphorin (Sema) signaling families, two families of receptor ligands involved in contact-repulsion mechanisms (30, 31) (fig. S7, A and B) that are also expressed in vOPCs (7). We next tested whether these signaling pathways underlie unidirectional contact repulsion in cocultures of preoptic area and medial ganglionic eminence explants containing GFP⁺ first-wave vOPCs and Tom⁺ interneurons, respectively. We showed that the pharmacological blockade of type a and b Eph receptor families with 200 μM of the competitive and reversible ligand lithocholic acid (32) did not affect unidirectional contact repulsion (Fig. 4O and fig. S7C). Therefore, we investigated whether Plxn-Sema signaling underlies unidirectional contact repulsion by knocking down simultaneously several Plxn members (Plxn1, a2, a3, b1, and b2) with expression of a small interfering RNA (siRNA) pool in interneurons. Unidirectional contact repulsion was largely impaired upon expression of the Plxn siRNA

pool (90.90% of the first-wave vOPC-interneuron contacts) compared with its control (fig. S7, D and E). While testing the involvement of each individual Plxn in unidirectional contact repulsion, we found that only targeting Plxna3 in interneurons abolished unidirectional contact repulsion (15.40%; Fig. 5, A to D, and fig. S7, F to K). We observed that the knockdown of Plxnb2 induced growth cone retraction without unidirectional contact repulsion (fig. S7L). Analysis of bulk RNA sequencing from first-wave vOPCs (7) revealed expression of several Semas (table S2). To identify the Sema(s) expressed by first-wave vOPCs that would partner with Plxna3 in unidirectional contact repulsion, we excluded secreted Semas and focused our analysis on transmembrane class 5 and 6 Semas, which are known receptors for a-class Plxns (33). The analysis of GFP⁺ first-wave vOPCs FACS-isolated from E13.5 *Sox10:GFP-DTA* embryos showed that messengers of all class 5 and 6 Semas are expressed by first-wave vOPCs (fig. S8A). We next tried to knock down these Semas in first-wave vOPCs by siRNAs or infection with short hairpin lentiviruses. Unfortunately, we were not able to transduce first-wave vOPCs. As an alternative, we used Neuro2A (N2A) cells, in which the endogenous expression of class 5 and 6 Semas is low (fig. S8, B to G). Accordingly, we detected unidirectional contact repulsion in a small fraction of E13.5 Tom⁺ interneurons that were cocultured with N2A cells (Fig. 5, E and H). The frequency of unidirectional contact repulsion was increased after overexpression of Sema6a and Sema6b (Fig. 5, F, G, I, and J), but not of other class 5 and 6 Semas, in N2A cells (fig. S8, H to K). By knocking down Plxna3 in interneurons, we demonstrated that the increase in unidirectional contact-repulsion frequency triggered upon Sema6a or Sema6b overexpression in N2A cells required endogenous expression of Plxna3 by interneurons (Fig. 5, K and L). This further suggests that a transient interaction between interneuron Plxna3 and first-wave vOPC Sema6a/6b drives unidirectional contact repulsion. To further test this hypothesis, we used blocking antibodies that recognize both Sema6a and Sema6b (Sema6a/6b; fig. S8, L to N) in coculture of interneurons and first-wave vOPCs, which dose-dependently abolished unidirectional contact repulsion (Fig. 5, M and N, and fig. S8O). At the subcellular level, we detected some enrichment of Plxna3 and Sema6a/6b signal in growth cones of interneurons and first-wave vOPCs, respectively (Fig. 5, O and P). Such subcellular location suggests that these molecules are important players to drive growth cone collapse and lead process retraction during unidirectional contact repulsion. We further investigated polarity reversal in interneurons by electroporating centrin-GFP and memb-Cherry. We observed a sequence during which the

growth cone of the leading process initiates retraction just before the regrowth of the new leading process at the opposite side, whereas the centrosome (centrin-GFP) initiates its migration later. Because the centrosome acts as microtubule organizing center (MTOC), our results suggest that microtubules are not initially involved in the growth of the new leading process after interacting with first-wave vOPCs or N2A cells overexpressing Sema6b (Fig. 5, Q and R, and movies S9 and S10). Altogether, our data demonstrate that unidirectional contact repulsion is driven by an interaction between Plxna3 and Sema6a/6b, further suggesting that first-wave vOPCs use a singular mechanism to signal to interneurons during development.

Discussion

Here, we provide a characterization of the migration pattern of first-wave vOPCs in the developing mouse brain. Despite being born in shared subpallial germinal regions, vOPCs and interneurons use distinct migration modes and occupy mutually exclusive forebrain territories while moving toward the cortex. Moreover, these cell types undergo saltatory migration characterized by different kinetics, and although vOPCs preferentially use blood vessels to move in the cortex, interneurons navigate in organized tangential streams. Among the important diffusible cues that guide neural migration in the cortex, the chemokine Cxcl12 attracts both interneurons and vOPCs. The Cxcl12 released by intermediate progenitors in the cortex marks a migratory stream that steers interneurons within the IZ or SVZ (21, 34). This chemokine is also secreted by forebrain blood vessels and attracts vOPCs (13). Whereas genetic ablation of interneurons does not affect the cortical distribution of vOPCs, loss of first-wave vOPCs impairs interneuron migration in the cortical wall, further suggesting that interneurons require first-wave vOPCs to properly navigate within the cerebral cortex. We showed that first-wave vOPC ablation increases the local availability of Cxcl12 in the vicinity of blood vessels to which interneurons are then attracted, thereby altering their progression toward the cortex. Because both cell types are responsive to Cxcl12, we postulated that an active mechanism carried on by first-wave vOPCs prevents interneurons from migrating along blood vessels. Our live-imaging analysis indeed demonstrated that first- but not second-wave vOPCs perform unidirectional contact repulsion on interneurons, thus guiding them to prevent their interaction with blood vessels while contributing to their overall progression into the forebrain. This mode of contact repulsion with polarity reversal is specific to first-wave vOPC-interneuron pairs and distinct from self-repulsion, as previously described for OPCs themselves (35) and

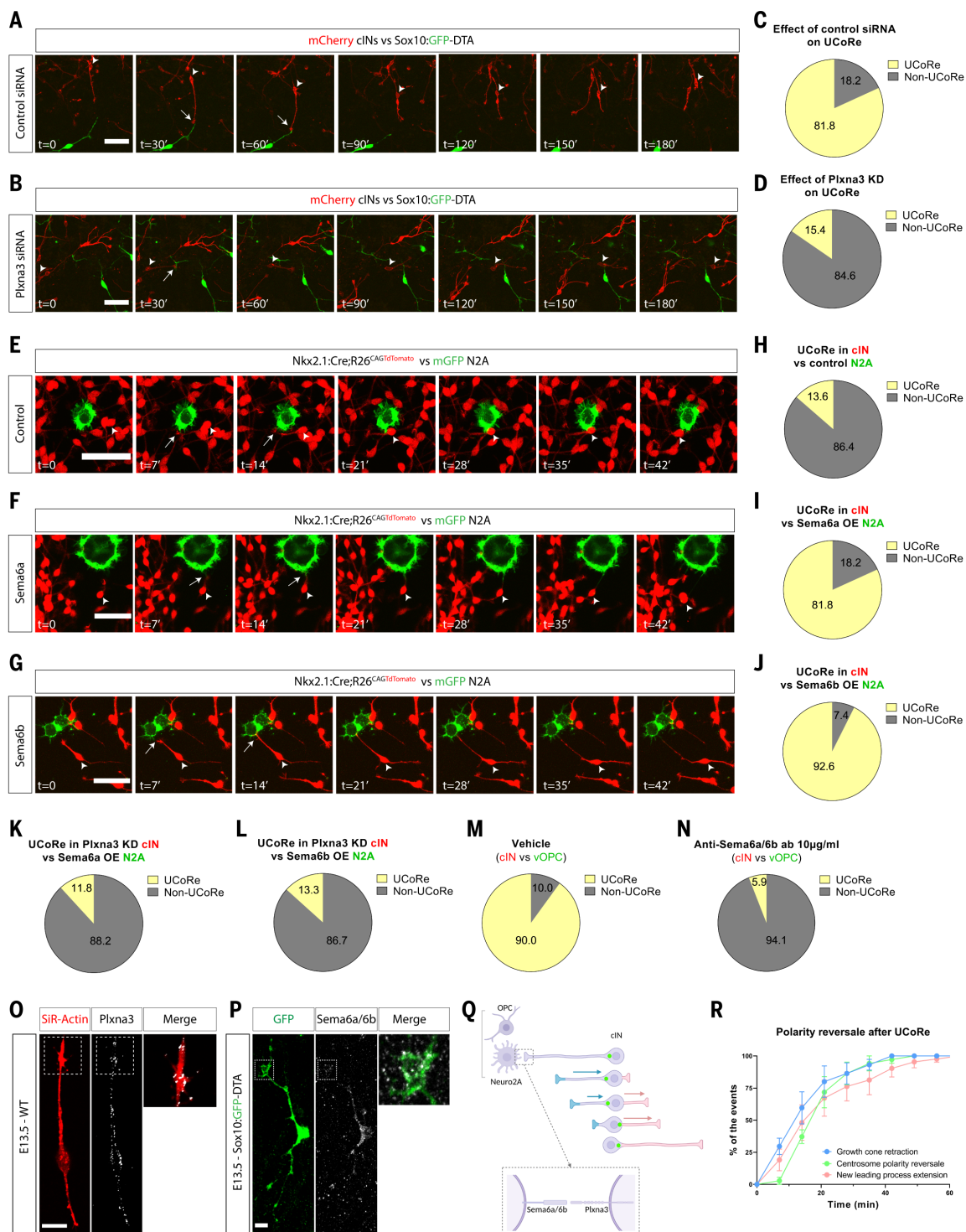


Fig. 5. Molecular mechanism underlying a UCoRe. (A and B) Time-lapse sequences illustrating the behavior of an interneuron (memb-Cherry, red) electroporated with control siRNA [(A); UCoRe] or Plxna3 siRNA (B; non-UCoRe), after contacting a first-wave vOPC (green). White arrows indicate contacts between interneuron and first-wave vOPC. Arrowheads track the soma of the interneuron of interest. (C and D) Pie charts reporting the fraction of interneurons undergoing UCoRe or non-UCoRe upon contacting first-wave vOPCs, as illustrated by (A) and (B) ($n = 11$ to 13 cells; $**P = 0.0031$, Fisher's exact test). (E to G) Time-lapse sequences illustrating the behavior of interneurons ($TdTomato^+$, red), after contacting N2A cells (green) overexpressing mGFP (control, E; non-UCoRe).

Sema6a [(F); UCoRe] or Sema6b plasmids [(G); UCoRe]. White arrows indicate contact between an interneuron and a N2A cell. Arrowheads track the soma of the interneuron of interest. (H to J) Pie charts reporting the fraction of interneurons undergoing UCoRe or non-UCoRe upon contacting N2A cells, as illustrated by (E), (F), and (G) ($n = 22$ to 27 cells; $****P < 0.0001$, Fisher's exact test). (K and L) Pie charts reporting the fraction of interneurons (memb-Cherry, red) undergoing UCoRe or non-UCoRe after electroporation with Plxna3 siRNA and upon contact with N2A cells overexpressing Sema6a (K) or Sema6b plasmids (L) ($n = 15$ to 17 cells; $****P < 0.0001$, Fisher's exact test). (M and N) Pie charts reporting the fraction of interneurons ($TdTomato^+$, red) undergoing UCoRe or non-UCoRe upon contact with

first-wave vOPCs (green) while being incubated with vehicle (M) or 10 µg/ml of anti-Sema6b antibody (N) ($n = 10$ to 17 cells; $****P < 0.0001$, Fisher's exact test). (O) Immunolabeling of an interneuron (SiR-Actin, red) and Plxna3 (white). Nuclei were counterstained with DAPI (blue). (P) Immunolabeling of a first-wave vOPC (GFP⁺, green) and Sema6a/6b (white). Nuclei were counterstained with DAPI (blue). Merges are the corresponding squared

regions. (Q) Scheme of UCoRe sequence when an interneuron contacts a first-wave vOPC or a N2A cell overexpressing Sema6a or Sema6b. Growth cone retraction is in blue, centrosome (or MTOC) in green, and the extending new leading process in red. (R) Graph showing the order and timing of UCoRe sequence. Scale bars: (O) and (P), 10 µm; (A), (B), (E), (F), and (G), 50 µm. KD, knockdown; OE, overexpression.

Cajal-Retzius cells (36, 37). Unidirectional contact repulsion on interneurons involves a sequence of events that starts with the growth cone collapse of their leading process and its retraction, followed by the regrowth of a new leading process at the opposite side of the cell body. We observed that centrosome migration (which acts as a MTOC) from the base of the disassembling leading process to the base of the new one occurs after growth initiation of the new process. This suggests that growth initiation of the leading process is independent of nucleation and polymerization of microtubules from the MTOC. At the molecular level, we identified that an atypical interaction between Plxna3 and Sema6a/6b expressed by interneurons and first-wave vOPCs, respectively, triggers a signaling pathway promoting unidirectional contact repulsion. Our attempt to detect a physical interaction between these molecules by coimmunoprecipitation on extracts from cocultured N2A cells transfected with either Plxna3 or Sema6b was unsuccessful, likely because such interaction is short (<10 min, as reported in Fig. 5R). Moreover, the nature of the intracellular cascade activated in interneurons upon first-wave vOPC interaction remains to be clarified. The reduction of interneuron number in the cortex upon first-wave vOPC depletion is still observed just before birth, an age during which second-wave vOPCs are actively migrating. This suggests that second-wave vOPCs cannot rescue the migration of interneurons, which is further supported by the demonstration that second-wave vOPCs do not perform unidirectional contact repulsion to most homochronic interneurons. We observed that interneuron depletion does not have a significant impact on the generation, survival, and migration of first- and second-wave vOPCs. However, by releasing factors such as Sonic hedgehog and fraktaline, interneurons control the generation of dorsally born OPCs (16, 38). This is another example suggesting that interneuron-OPC cross-talk varies spatially and temporally. Some first-wave vOPCs and interneurons establish specific interaction to form transient synapses at early postnatal stages and later engage in myelination of specific local circuits (5, 11). However, most first-wave vOPCs die before postnatal day 10 (11). Therefore, by showing that first-wave vOPCs support the migration of interneurons in the developing cerebral cortex, our work identifies a noncanonical and transient role for first-wave vOPCs. Furthermore, whereas unidirectional contact repul-

sion occurs during development between pairs of interneurons and first-wave vOPCs, some pairs must express mutual recognition molecular codes after birth to promote longer-term interaction for the formation of transient synapses and later axon myelination.

Our results show that despite being less numerous, first-wave vOPCs support the migration of interneurons across cortical territories by using unidirectional contact repulsion. This mechanism allows both cell populations to adopt specific migration patterns in the cortex while also being attracted by Cx12. Blood vessels are found throughout the cortical wall and are indeed an important source of Cxcl12 that, if not covered and consumed by first-wave vOPCs, may affect interneuron migration by interfering with the existing cortical IZ and MZ Cxcl12 gradients generated by intermediate progenitors and meningeal cells, respectively (21, 39). Unidirectional contact repulsion contributes to the guidance of interneurons as the cortex matures and gets more perfused by blood vessels, which are a source of Cxcl12 release.

Methods summary

Genetic mouse models were used to visualize or deplete either vOPCs or interneurons. First-wave vOPC progenies were analyzed at E13.5 in Nkx2.1:Cre; R26^{CAGTdTmato} and Dbx1:Cre; R26^{CAGTdTmato} mouse models. Sox10:GFP-DTA and Dlx5,6:Cre-GFP E13.5 and E16.5 brains were processed into organotypic slices to track the migration of vOPCs and cortical interneurons, respectively. Brains from Sox10:GFP-DTA, Sox10:Venus, Nkx2.1:Cre; R26^{CAGTdTmato}, and Dlx5,6:Cre-GFP; R26^{CAGTdTmato} mice were microdissected into explants and cultured to analyze unidirectional contact repulsion between vOPCs and interneurons. Sox10:GFP-DTA females were crossed with either Pdgfr α :Cre^{ERT} or Dlx5,6:CreGFP; Pdgfr α :Cre^{ERT} males to deplete first-wave vOPCs after intraperitoneal injections of tamoxifen at E11.5 and E12.5. A model of interneuron depletion was generated by breeding R26:DTA females with Dlx5,6:Cre-GFP males.

For all histological analyses, embryonic heads or brains were fixed in 4% paraformaldehyde overnight at 4°C and then cryopreserved in a 20% sucrose solution diluted in phosphate-buffered saline (PBS) overnight at 4°C. Brains were then frozen in optimal cutting temperature medium and kept at -80°C until cryostat cutting. Brain slices were permeabilized, blocked in PBS/0.3% Triton X-100/10% donkey serum,

and then incubated overnight at 4°C with primary antibodies diluted in PBS/0.3% Triton X-100/1% donkey serum. After three rinses with PBS/0.3% Triton X-100/5% donkey serum, slices were incubated in the same solution containing secondary antibodies for 2 hours at room temperature. Images were obtained using an inverted confocal microscope (Nikon AI).

Organotypic slice cultures from embryonic brains were used to study the migration of vOPCs and cortical interneurons. Brains were processed into 300-µm coronal slices and harvested on a Milliecell(Millipore) culture insert placed on glass-bottomed dishes. Dishes were filled with neurobasal medium supplemented in B27, N2, and glutamine. Slices were kept in a humidified incubator saturated with 5% CO₂ for a maximum of 8 hours before time-lapse recording. IsolectinB4 was added on top of organotypic slices to stain blood vessels. For every treatment (Cxcl11 Ab, Cxcl12 Ab, or XAV939), molecules were added on top of organotypic slices as well. Time-lapse acquisitions were obtained every 5 min for at least 5 hours using an inverted confocal microscope. Analyses of migration parameters were performed using the mTrackJ plugin in Fiji.

Study of vOPC-interneuron interaction was performed in a two-dimensional culture of primary vOPCs and interneurons. These cultures were generated by placing microdissected ganglionic eminence and preoptic area explants on top of a homochronic cortical feeder. Briefly, glass-bottomed dishes were coated with poly-ornithine and laminin. The feeder layer of cortical cells was prepared by mechanical dissociation of either E13.6 or E16.5 wild-type cortices in supplemented neurobasal medium. The dissociated cells were plated in coated glass-bottomed dishes and left to adhere for 2 hours at 37°C in a humidified incubator saturated with 5% CO₂. The next day, ganglionic eminence or preoptic area explants of ~300 µm were then plated on top of the cortical feeder layer. To knock down Plexins in interneurons at E13.5, ex vivo electroporation of medial ganglionic eminences was performed before microdissecting the explants. For analyses of contact repulsion between vOPCs and interneurons, time-lapse acquisitions were obtained every 5 min for at least 10 hours using an inverted confocal microscope.

REFERENCE AND NOTES

- K. A. Nave. Myelination and the trophic support of long axons. *Nat. Rev. Neurosci.* **11**, 275–283 (2010). doi: 10.1038/nrn2797; pmid: 20216548

2. A. M. Ravanelli *et al.*, Sequential specification of oligodendrocyte lineage cells by distinct levels of Hedgehog and Notch signaling. *Dev. Biol.* **444**, 93–106 (2018). doi: [10.1016/j.ydbio.2018.10.004](https://doi.org/10.1016/j.ydbio.2018.10.004); pmid: [30347186](https://pubmed.ncbi.nlm.nih.gov/30347186/)
3. D. E. Bergles, J. D. Roberts, P. Somogyi, C. E. Jahr, Glutamatergic synapses on oligodendrocyte precursor cells in the hippocampus. *Nature* **405**, 187–191 (2000). doi: [10.1038/35012083](https://doi.org/10.1038/35012083); pmid: [10821275](https://pubmed.ncbi.nlm.nih.gov/10821275/)
4. S. C. Lin, D. E. Bergles, Synaptic signaling between GABAergic interneurons and oligodendrocyte precursor cells in the hippocampus. *Nat. Neurosci.* **7**, 24–32 (2004). doi: [10.1038/nn1162](https://doi.org/10.1038/nn1162); pmid: [14661022](https://pubmed.ncbi.nlm.nih.gov/14661022/)
5. D. Ordúz *et al.*, Interneurons and oligodendrocyte progenitors form a structured synaptic network in the developing neocortex. *eLife* **4**, e06953 (2015). doi: [10.7554/eLife.06953](https://doi.org/10.7554/eLife.06953); pmid: [25902404](https://pubmed.ncbi.nlm.nih.gov/25902404/)
6. S. Marques *et al.*, Oligodendrocyte heterogeneity in the mouse juvenile and adult central nervous system. *Science* **352**, 1326–1329 (2016). doi: [10.1126/science.aaf463](https://doi.org/10.1126/science.aaf463); pmid: [27284195](https://pubmed.ncbi.nlm.nih.gov/27284195/)
7. S. Marques *et al.*, Transcriptional convergence of oligodendrocyte lineage progenitors during development. *Dev. Cell* **46**, 504–517.e7 (2018). doi: [10.1016/j.devcel.2018.07.005](https://doi.org/10.1016/j.devcel.2018.07.005); pmid: [30078729](https://pubmed.ncbi.nlm.nih.gov/30078729/)
8. N. Kessaris *et al.*, Competing waves of oligodendrocytes in the forebrain and postnatal elimination of an embryonic lineage. *Nat. Neurosci.* **9**, 173–179 (2006). doi: [10.1038/nn1620](https://doi.org/10.1038/nn1620); pmid: [16388308](https://pubmed.ncbi.nlm.nih.gov/16388308/)
9. M. A. Petryniak, G. B. Potter, D. H. Rowitch, J. L. Rubenstein, Dlx1 and Dlx2 control neuronal versus oligodendroglial cell fate acquisition in the developing forebrain. *Neuron* **55**, 417–433 (2007). doi: [10.1016/j.neuron.2007.06.036](https://doi.org/10.1016/j.neuron.2007.06.036); pmid: [17678855](https://pubmed.ncbi.nlm.nih.gov/17678855/)
10. J. C. Silbereis *et al.*, Olig1 function is required to repress dlx1/2 and interneuron production in Mammalian brain. *Neuron* **81**, 574–587 (2014). doi: [10.1016/j.neuron.2013.11.024](https://doi.org/10.1016/j.neuron.2013.11.024); pmid: [24507192](https://pubmed.ncbi.nlm.nih.gov/24507192/)
11. D. Ordúz *et al.*, Developmental cell death regulates lineage-related interneuron-oligodendroglial functional clusters and oligodendrocyte homeostasis. *Nat. Commun.* **10**, 4249 (2019). doi: [10.1038/s41467-019-11904-4](https://doi.org/10.1038/s41467-019-11904-4); pmid: [31534164](https://pubmed.ncbi.nlm.nih.gov/31534164/)
12. S. A. Anderson, D. D. Eisenstat, L. Shi, J. L. Rubenstein, Interneuron migration from basal forebrain to neocortex: Dependence on Dlx genes. *Science* **278**, 474–476 (1997). doi: [10.1126/science.278.5337.474](https://doi.org/10.1126/science.278.5337.474); pmid: [9334308](https://pubmed.ncbi.nlm.nih.gov/9334308/)
13. H. H. Tsai *et al.*, Oligodendrocyte precursors migrate along vasculature in the developing nervous system. *Science* **351**, 379–384 (2016). doi: [10.1126/science.aad3839](https://doi.org/10.1126/science.aad3839); pmid: [26798014](https://pubmed.ncbi.nlm.nih.gov/26798014/)
14. S. A. Anderson, O. Marín, C. Horn, K. Jennings, J. L. Rubenstein, Distinct cortical migrations from the medial and lateral ganglionic eminences. *Development* **128**, 353–363 (2001). doi: [10.1242/dev.128.3.353](https://doi.org/10.1242/dev.128.3.353); pmid: [11152634](https://pubmed.ncbi.nlm.nih.gov/11152634/)
15. G. Zimmer *et al.*, Bidirectional ephrinB3/EphA4 signaling mediates the segregation of medial ganglionic eminence- and preoptic area-derived interneurons in the deep and superficial migratory stream. *J. Neurosci.* **31**, 18364–18380 (2011). doi: [10.1523/JNEUROSCI.4690-11.2011](https://doi.org/10.1523/JNEUROSCI.4690-11.2011); pmid: [22171039](https://pubmed.ncbi.nlm.nih.gov/22171039/)
16. A. Voronova *et al.*, Migrating interneurons secrete fractalkine to promote oligodendrocyte formation in the developing mammalian brain. *Neuron* **94**, 500–516.e9 (2017). doi: [10.1016/j.neuron.2017.04.018](https://doi.org/10.1016/j.neuron.2017.04.018); pmid: [28472653](https://pubmed.ncbi.nlm.nih.gov/28472653/)
17. C. Lange *et al.*, Relief of hypoxia by angiogenesis promotes neural stem cell differentiation by targeting glycolysis. *EMBO J.* **35**, 924–941 (2016). doi: [10.15252/embj.201592372](https://doi.org/10.15252/embj.201592372); pmid: [26856890](https://pubmed.ncbi.nlm.nih.gov/26856890/)
18. M. Barber *et al.*, Vascular-derived Vegfa promotes cortical interneuron migration and proximity to the vasculature in the developing forebrain. *Cereb. Cortex* **28**, 2577–2593 (2018). doi: [10.1093/cercor/bhy082](https://doi.org/10.1093/cercor/bhy082); pmid: [29901792](https://pubmed.ncbi.nlm.nih.gov/29901792/)
19. S. Minocha *et al.*, NG2 glia are required for vessel network formation during embryonic development. *eLife* **4**, e09102 (2015). doi: [10.7554/eLife.09102](https://doi.org/10.7554/eLife.09102); pmid: [26651999](https://pubmed.ncbi.nlm.nih.gov/26651999/)
20. N. Flames *et al.*, Short- and long-range attraction of cortical GABAergic interneurons by neuregulin-1. *Neuron* **44**, 251–261 (2004). doi: [10.1016/j.neuron.2004.09.028](https://doi.org/10.1016/j.neuron.2004.09.028); pmid: [15473965](https://pubmed.ncbi.nlm.nih.gov/15473965/)
21. M. C. Tiveron *et al.*, Molecular interaction between projection neuron precursors and invading interneurons via stromal-derived factor 1 (CXCL12)/CXCR4 signaling in the cortical subventricular zone/intermediate zone. *J. Neurosci.* **26**, 13273–13278 (2006). doi: [10.1523/JNEUROSCI.4162-06.2006](https://doi.org/10.1523/JNEUROSCI.4162-06.2006); pmid: [17182777](https://pubmed.ncbi.nlm.nih.gov/17182777/)
22. G. López-Bendito *et al.*, Chemokine signaling controls intracortical migration and final distribution of GABAergic interneurons. *J. Neurosci.* **28**, 1613–1624 (2008). doi: [10.1523/JNEUROSCI.4651-07.2008](https://doi.org/10.1523/JNEUROSCI.4651-07.2008); pmid: [18272682](https://pubmed.ncbi.nlm.nih.gov/18272682/)
23. L. Kurmann *et al.*, Transcriptomic analysis of human brain-microvascular endothelial response to pericytes: Cell orientation defines barrier function. *Cells* **10**, 963 (2021). doi: [10.3390/cells10040963](https://doi.org/10.3390/cells10040963); pmid: [33924251](https://pubmed.ncbi.nlm.nih.gov/33924251/)
24. Y. Zhang *et al.*, An RNA-sequencing transcriptome and splicing database of glia, neurons, and vascular cells of the cerebral cortex. *J. Neurosci.* **34**, 11929–11947 (2014). doi: [10.1523/JNEUROSCI.1860-14.2014](https://doi.org/10.1523/JNEUROSCI.1860-14.2014); pmid: [25186741](https://pubmed.ncbi.nlm.nih.gov/25186741/)
25. P. Abe *et al.*, CXCR7 prevents excessive CXCL12-mediated downregulation of CXCR4 in migrating cortical interneurons. *Development* **141**, 1857–1863 (2014). doi: [10.1242/dev.104224](https://doi.org/10.1242/dev.104224); pmid: [24718993](https://pubmed.ncbi.nlm.nih.gov/24718993/)
26. U. Naumann *et al.*, CXCR7 functions as a scavenger for CXCL12 and CXCL11. *PLOS ONE* **5**, e9175 (2010). doi: [10.1371/journal.pone.0009175](https://doi.org/10.1371/journal.pone.0009175); pmid: [20161793](https://pubmed.ncbi.nlm.nih.gov/20161793/)
27. Y. Wang *et al.*, CXCR4 and CXCR7 have distinct functions in regulating interneuron migration. *Neuron* **69**, 61–76 (2011). doi: [10.1016/j.neuron.2010.12.005](https://doi.org/10.1016/j.neuron.2010.12.005); pmid: [21220099](https://pubmed.ncbi.nlm.nih.gov/21220099/)
28. C. G. Silva *et al.*, Cell-intrinsic control of interneuron migration drives cortical morphogenesis. *Cell* **172**, 1063–1078.e19 (2018). doi: [10.1016/j.cell.2018.01.031](https://doi.org/10.1016/j.cell.2018.01.031); pmid: [29474907](https://pubmed.ncbi.nlm.nih.gov/29474907/)
29. H. Mi *et al.*, PANTHER version 16: A revised family classification, tree-based classification tool, enhancer regions and extensive API. *Nucleic Acids Res.* **49** (D1), D394–D403 (2021). doi: [10.1093/nar/gkaa1106](https://doi.org/10.1093/nar/gkaa1106); pmid: [33290554](https://pubmed.ncbi.nlm.nih.gov/33290554/)
30. L. T. Alto, J. R. Terman, Semaphorins and their signaling mechanisms. *Methods Mol. Biol.* **1493**, 1–25 (2017). doi: [10.1007/978-1-4939-6448-2_1](https://doi.org/10.1007/978-1-4939-6448-2_1); pmid: [27787839](https://pubmed.ncbi.nlm.nih.gov/27787839/)
31. A. Kania, R. Klein, Mechanisms of ephrin-Eph signalling in development: physiology and disease. *Nat. Rev. Mol. Cell Biol.* **17**, 240–256 (2016). doi: [10.1038/nrm.2015.16](https://doi.org/10.1038/nrm.2015.16); pmid: [26790531](https://pubmed.ncbi.nlm.nih.gov/26790531/)
32. C. Giorgio *et al.*, Lithocholic acid is an Eph-Ephrin ligand interfering with Eph-kinase activation. *PLOS ONE* **6**, e18128 (2011). doi: [10.1371/journal.pone.0018128](https://doi.org/10.1371/journal.pone.0018128); pmid: [21479221](https://pubmed.ncbi.nlm.nih.gov/21479221/)
33. R. J. Pasterkamp, Getting neural circuits into shape with semaphorins. *Nat. Rev. Neurosci.* **13**, 605–618 (2012). doi: [10.1038/nrn3302](https://doi.org/10.1038/nrn3302); pmid: [22895477](https://pubmed.ncbi.nlm.nih.gov/22895477/)
34. A. Sessa *et al.*, Tbr2-positive intermediate (basal) neuronal progenitors safeguard cerebral cortex expansion by controlling amplification of pallial glutamatergic neurons and attraction of subpallial GABAergic interneurons. *Genes Dev.* **24**, 1816–1826 (2010). doi: [10.1101/gad.575410](https://doi.org/10.1101/gad.575410); pmid: [20713522](https://pubmed.ncbi.nlm.nih.gov/20713522/)
35. E. G. Hughes, S. H. Kang, M. Fukaya, D. E. Bergles, Oligodendrocyte progenitors balance growth with self-repulsion to achieve homeostasis in the adult brain. *Nat. Neurosci.* **16**, 668–676 (2013). doi: [10.1038/nn.3390](https://doi.org/10.1038/nn.3390); pmid: [23624515](https://pubmed.ncbi.nlm.nih.gov/23624515/)
36. M. Barber *et al.*, Migration speed of Cajal-Retzius cells modulated by vesicular trafficking controls the size of higher-order cortical areas. *Curr. Biol.* **25**, 2466–2478 (2015). doi: [10.1016/j.cub.2015.08.028](https://doi.org/10.1016/j.cub.2015.08.028); pmid: [26387718](https://pubmed.ncbi.nlm.nih.gov/26387718/)
37. V. Villar-Cerviño *et al.*, Contact repulsion controls the dispersion and final distribution of Cajal-Retzius cells. *Neuron* **77**, 457–471 (2013). doi: [10.1016/j.neuron.2012.11.023](https://doi.org/10.1016/j.neuron.2012.11.023); pmid: [23395373](https://pubmed.ncbi.nlm.nih.gov/23395373/)
38. C. C. Winkler *et al.*, The dorsal wave of neocortical oligodendrogenesis begins embryonically and requires multiple sources of Sonic Hedgehog. *J. Neurosci.* **38**, 5237–5250 (2018). doi: [10.1523/JNEUROSCI.3392-17.2018](https://doi.org/10.1523/JNEUROSCI.3392-17.2018); pmid: [29739868](https://pubmed.ncbi.nlm.nih.gov/29739868/)
39. V. Borrell, O. Marín, Meninges control tangential migration of hem-derived Cajal-Retzius cells via CXCL12/CXCR4 signaling. *Nat. Neurosci.* **9**, 1284–1293 (2006). doi: [10.1038/nn1764](https://doi.org/10.1038/nn1764); pmid: [16964252](https://pubmed.ncbi.nlm.nih.gov/16964252/)

ACKNOWLEDGMENTS

We thank E. Huillard (Sox10:GFP-DTA), H. Okano (Sox10:Venus), R. Franzen (Pdgfra:Cre^{ERT2}), and A. Pierani (Dbx1:Cre) for providing transgenic mouse lines; A. Püschel (Sema6a-Flag, Sema6c-Flag, Sema5a-Flag, Sema5b-Flag), L. Tamagnone (Sema6b-Myc, Sema6d-V5His), I. Caillé (centrin-GFP), and A. Chédotal (Sema6a) for providing plasmids; M. C. Angulo, A. Pierani, L. Tamagnone, and S. Cappello for providing feedback on the manuscript, as well as all the members of the Nguyen laboratory for their input; and S. Ormenese, A. Hego, C. Vanwinge, and R. Stephan from the GIGA-Cell Imaging and flow cytometry platforms and D. Bawir from the GIGA-proteomics platform for technical support. All drawings were created with BioRender.com. **Funding:** This work was supported by the Fonds de la Recherche Scientifique (FRS) – Fonds National de la Recherche Scientifique (FNRS) (Synet: Excellence of Science grant no. 0019118F-RG36), the Fonds Leon Fredericq, the Fondation Médicale Reine Elisabeth, the Fondation Simone et Pierre Clerdent, the Belgian Science Policy (IAP VII network P7/20), the ERANET Neuron (STEM-MCD and NeuroTalk), and the Win2Wal (ChipOmics; no. 2010126). F.L. is a Fonds pour la Formation à la Recherche dans l’Industrie et dans l’Agriculture (FRIA) doctoral fellow, M.J.-T. and J.S. are postdoctoral researchers, C.G.S. is an EOS postdoctoral fellow, and L.N. is research director at the FRS-FNRS. **Author contributions:** C.G.S. and L.N. conceptualized and supervised the study. F.L. designed, conceptualized, performed, and analyzed most experiments. J.S. designed, performed, and analyzed experiments to investigate the molecular mechanisms of unidirectional contact repulsion. M.J.-T. designed, performed, and analyzed molecular biology and biochemical experiments. G.M. performed proteomic analysis. F.L., C.G.S., and L.N. wrote the manuscript with input from all authors. **Competing interests:** The authors declare no competing interests. **Data and materials availability:** All annotated data are available from the ProteomeXchange Consortium in the Proteomics Identification Database (PRIDE accession no. PXD031876). All other data are available in the main text or the supplementary materials. **License information:** Copyright © 2022 the authors, some rights reserved; exclusive licensee American Association for the Advancement of Science. No claim to original US government works. <https://www.science.org/about/science-licenses-journal-article-reuse>

SUPPLEMENTARY MATERIALS

science.org/doi/10.1126/science.abn6204

Materials and Methods

Figs. S1 to S8

Tables S1 to S4

References (40–48)

MDAR Reproducibility Checklist

Movies S1 to S10

[View/request a protocol for this paper from Bio-protocol.](https://www.bio-protocol.org)

Submitted 8 December 2021; accepted 5 April 2022
10.1126/science.abn6204